The complex band structure for armchair graphene nanoribbons*

Zhang Liu-Jun(张留军)† and Xia Tong-Sheng(夏同生)

School of Electronic Information Engineering, Beijing University of Aeronautics and Astronautics, Beijing 100191, *China*

(Received 20 May 2010; revised manuscript received 28 May 2010)

Using a tight binding transfer matrix method, we calculate the complex band structure of armchair graphene nanoribbons. The real part of the complex band structure calculated by the transfer matrix method fits well with the bulk band structure calculated by a Hermitian matrix. The complex band structure gives extra information on carrier's decay behaviour. The imaginary loop connects the conduction and valence band, and can profoundly affect the characteristics of nanoscale electronic device made with graphene nanoribbons. In this work, the complex band structure calculation includes not only the first nearest neighbour interaction, but also the effects of edge bond relaxation and the third nearest neighbour interaction. The band gap is classified into three classes. Due to the edge bond relaxation and the third nearest neighbour interaction term, it opens a band gap for $N = 3M-1$. The band gap is almost unchanged for $N = 3M+1$, but decreased for $N = 3M$. The maximum imaginary wave vector length provides additional information about the electrical characteristics of graphene nanoribbons, and is also classified into three classes.

Keywords: armchair graphene nanoribbons, complex band structure, edge bond relaxation, third nearest neighbour interaction

PACC: 7125X, 7125, 7115

1. Introduction

In the quest for nanoscale devices, carbon nanotubes and graphene show promising aspects for the application in nanoelectronic system. They have very high carrier mobility and are thus considered as alternative materials to silicon.[1−3] However, the chirality of carbon nanotubes is difficult to control and the structure can not readily be integrated into an electronic system in practice. Not just carbon nanotubes, the metallic property of graphene sheet limits its application to semiconductor devices. Graphene nanoribbons (GNRs), a narrow ribbon cutting from graphene sheet, is a quasi-1D material with a band gap (the band gap relies on the width of the nanoribbon and their crystallo-graphic direction),[4−6] and have attracted a lot of research interest.

We know that band structure is one of the most fundamental properties for all semiconductor materials. Many models are proposed to study the band structure of GNRs.[7−11] Simple tight binding model shows that there are mainly two kinds of GNRs: the armchair and zigzag ones.[10] The zigzag ones exhibit edge-localised states and are metallic. While armchair nanoribbons have no edge-localised states and could be semiconductor material.[8,12,13] Including only the first nearest neighbour interaction, the simple tight binding calculations have shown that, for armchair nanoribbon, when $N = 3M - 1$ (N is the atomic number in the width direction, and M is an integer), the GNRs is metallic, otherwise, it is semiconductor.[10,14] However, recent models find that distortion can convert these armchair metallic nanoribbons into semiconductors. More recently, it is discovered that there are band gaps in all armchair nanoribbons even without distortion due to the third nearest neighbour carbon–carbon interactions. The existence of band gaps in all armchair nanoribbons has been also confirmed by independent first-principle local-density-functional (LDF) calculations.[8,9,15] Therefore, a complete tight binding model scheme for the band structure calculations should include the edge bond relaxation and the third nearest neighbour interaction.[14]

These studies are all carried out on the modeling of the real part of the band structure for GNRs; however, a complete band structure calculation of the band structure should also include its imaginary part. One can split the wave vector into a part parallel to the interface of interest, $\boldsymbol{k}_{//}$, and a part perpendicu-

*Project supported by the Fundamental Research Funds for the Central Universities (Grant No. YWF-10-02-040).

†Corresponding author. E-mail: zhangliujun@ee.buaa.edu.cn

© 2010 Chinese Physical Society and IOP Publishing Ltd

lar to the interface $\boldsymbol{k}_z$. For each real $\boldsymbol{k}_{//}$, one can find the dispersion relations $E = E(\boldsymbol{k}_z)$, allowing complex $\boldsymbol{k}_z = p + \mathrm{i}q$.[16−20] The energy bands corresponding to complex $\boldsymbol{k}$ vectors are called complex bands. It has been studied in the last several decades to understand the electronic behaviour of surface states, and devices having quantum well or superlattice structure. More recently the complex band structure is applied to study the leakage performance of nanoscale transistors.[21,22] Assuming a particle tunnels through a barrier, the imaginary part of the complex band structure describes the spatially decaying behaviour of the wave function. We denote the imaginary part q as the decay parameter; the corresponding wave function will fall off as $\sim \mathrm{e}^{-qz}$. The imaginary $\boldsymbol{k}_z$ region of the complex band structure determines how an electron with a given energy will tunnel through a crystal.[16,20] And as discussed in early works, the imaginary part of the complex band structure forms a loop connecting the conduction and valence band and describes the evanescent behaviour of the band gap states.[16−20] The present work will have the major thrust on calculating the full complex band structure of GNRs using a tight binding transfer matrix method, rather than a simple Hermitian matrix for real band structure modeling. The lattice will be treated as a slab, and the edge bond relaxation and the third nearest neighbour interaction will be included.[14−19,21,22]

In Section 2, we discuss the complex band structure calculations of armchair GNRs by a tight binding transfer matrix method. The complex band structure is analysed in detail in Section 3. Conclusions are then drawn in Section 4.

2. Theory of complex band structure calculations

Most researchers have employed the slab lattice layer geometry, and the complex band structure is then calculated by expanding the eigenvectors in the planar orbital basis with in plane wave vector $\boldsymbol{k}_{//}$.[23−27] The tight binding transfer matrix method gives a most intuitive way to calculate the complex band structure, and has already been used to calculate the complex band structure of Si and carbon nanotubes.[21,22]

Figure 1(a) shows the general lattice structure of an armchair GNRs ($\boldsymbol{k}_x = \boldsymbol{k}_{//}$). Since GNRs have finite dimension in $\boldsymbol{k}_x$ direction, it will be taken as a one dimensional chain as shown in Fig. 1(b). The squares marked by 1 or 2 are the atomic layers of the armchair GNRs. Every two atomic layers, 1 and 2, form one sublayer, and every two sublayers, A and B, form one superlayer.[28] The second nearest neighbour interaction, which only shifts the dispersion relation in energy direction, does not change the band-gap and is not included in our calculation. We will consider the first nearest neighbour and the third nearest neighbour atomic coupling with one π orbital for each atom. At the same time, the edge bond relaxation term is also included.

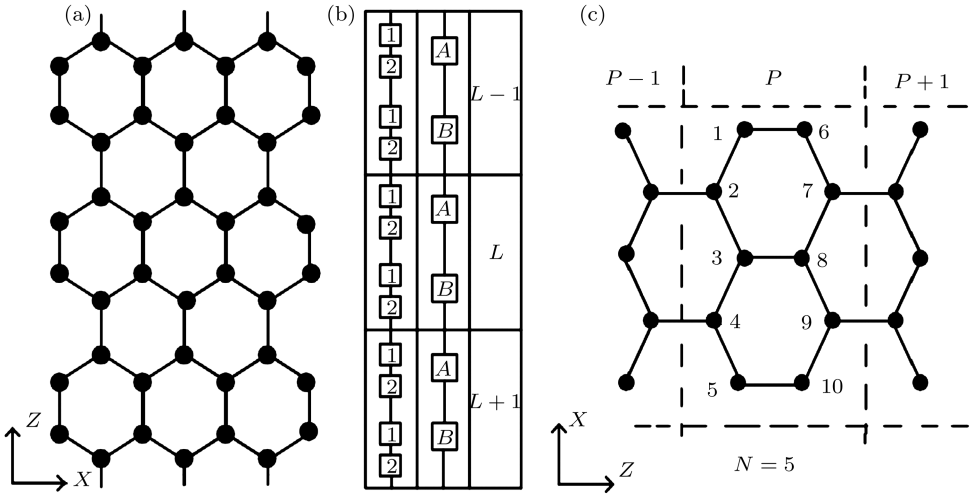


Fig. 1. (a) Schematic lattice structure of the armchair GNRs. (b) One-dimension chain representation of the schematic armchair GNRs lattice structure. The squars marked by 1 or 2 are the atomic layers of the armchair GNRs. Every two atomic layers, 1 and 2, forms one sublayer, and every two sublayers, A and B, forms one superlayer. (c) Lattice structure of an armchair GNRs, the width of the armchair GNRs is N. Every unit cell contains $2N$ atoms.

For complex band structure calculations, the wave function (ψ) of the whole system can be written as:[18,19,29]

$$|\psi\rangle = \frac{1}{\sqrt{N_n}} \sum_{L,\mu} C_{L,\mu} \sum_{\boldsymbol{R}_i} \mathrm{e}^{\mathrm{i}\boldsymbol{k}_{//}\cdot\boldsymbol{R}_i} |L,\mu,\boldsymbol{R}_i\rangle, \quad (1)$$

where L indexes the superlayers, μ denotes either sublayer A or B, $C_{L,\mu}$ is the expansion coefficients, $|L,\mu,\boldsymbol{R}_i\rangle$ is the ith atomic orbital in the μ sublayer and the L superlayer, $\boldsymbol{R}_i$ is a lattice vector, and N_n is the normalised coefficients. The Schrodinger equation $H|\psi\rangle = E|\psi\rangle$ for this system can be written as:

$$\begin{aligned} &H_{L,A}^{L,A} \times C_{L,A} + H_{L-1,B}^{L,A} \times C_{L-1,B} \\ &+ H_{L,B}^{L,A} \times C_{L,B} = 0, \\ &H_{L-1,B}^{L-1,B} \times C_{L-1,B} + H_{L-1,A}^{L-1,B} \times C_{L-1,A} \\ &+ H_{L,A}^{L-1,B} \times C_{L,A} = 0, \end{aligned} \quad (2)$$

where $C_{P,\mu}$ are column vectors, $P \in \{L, L-1\}$ and $\mu \in \{A, B\}$. The Bloch state in the μ sublayer and the L superlayer is written as: $\left|L,\mu,i,k_{//}\right\rangle$. The matrix element of the Hamiltonian between states $|P_1,\mu_1,i,k_x\rangle$ and $|P_2,\mu_2,j,k_x\rangle$is given by $\left[H_{P_2,\mu_2}^{P_1,\mu_1}\right]_{ij}$ and it can be written as:

$$\begin{aligned} &\left[H_{P_2,\mu_2}^{P_1,\mu_1}\right]_{ij} \\ &= \sum_{\boldsymbol{R}_{ij}} \mathrm{e}^{\mathrm{i}\boldsymbol{k}_{//}\cdot\boldsymbol{R}_{ij}} \langle P_1,\mu_1,\boldsymbol{R}_i| H |P_2,\mu_2,\boldsymbol{R}_j\rangle \end{aligned} \quad (3)$$

and

$$\langle P_1,\mu_1,\boldsymbol{R}_i| H |P_2,\mu_2,\boldsymbol{R}_j\rangle = \begin{cases} \underset{|\boldsymbol{R}_{ij}|=b}{\overset{(i,j)\in \text{edge bonds}}{\rightarrow}} r_1 + \Delta r, \\ \underset{|\boldsymbol{R}_{ij}|=c}{\overset{(i,j)\in \text{others}}{\rightarrow}} r_1, \\ \underset{\rightarrow}{} r_3, \end{cases} \quad (4)$$

where $d = \sqrt{3}a$, $c = 2b$, $a = \sqrt{3}b$, and b is the bonding length. r_1 and r_3 refer to the first nearest neighbour and the third nearest neighbour hopping parameters, respectively, and we use Δr as the correction to r_1 for the bonds due to edge bond relaxation effect.

For armchair GNRs, there are six $N \times N$ $H_{P_2,\mu_2}^{P_1,\mu_1}$ matrixes and we have:

$$H_{L-1,A}^{L-1,B} = (H_{L,B}^{L,A})^{+}, \quad (5)$$

$$H_{L,A}^{L-1,B} = (H_{L-1,B}^{L,A})^{+}. \quad (6)$$

From Eq. (2), it can be directly derived that:

$$\begin{aligned} \begin{bmatrix} C_{L,B} \\ C_{L,A} \end{bmatrix} = &\begin{bmatrix} -(H_{L,B}^{L,A})^{-1} H_{L,A}^{L,A} & -(H_{L,B}^{L,A})^{-1} H_{L-1,B}^{L,A} \\ I & 0 \end{bmatrix} \\ &\times \begin{bmatrix} -(H_{L,A}^{L-1,B})^{-1} H_{L-1,B}^{L-1,B} & -(H_{L,A}^{L-1,B})^{-1} H_{L-1,A}^{L-1,B} \\ I & 0 \end{bmatrix} \begin{bmatrix} C_{L-1,B} \\ C_{L-1,A} \end{bmatrix} \end{aligned} \quad (7)$$

and it has the relation:

$$\begin{bmatrix} C_{L,B} \\ C_{L,A} \end{bmatrix} = \mathrm{e}^{\mathrm{i}k_z d} \begin{bmatrix} C_{L-1,B} \\ C_{L-1,A} \end{bmatrix}. \quad (8)$$

The complex band structure of armchair GNRs can then be determined by substituting Hamiltonian into Eqs. (7) and (8).

Figure 1(c) shows the lattice structure used for calculating the bulk band structure.[10,29–31] The wave function of the whole system is :

$$|\psi\rangle = \frac{1}{\sqrt{N_n}} \sum_{P} \sum_{\boldsymbol{R}_{Pi}} \mathrm{e}^{\mathrm{i}\boldsymbol{k}\cdot\boldsymbol{R}_{Pi}} C_i |\varphi_i\rangle, \quad (9)$$

where the sum of i is over all the $2N$ atoms in a unit cell; the sum of P is over all the unit cells in one-dimension infinite system. $\boldsymbol{R}_{Pi}$ is the lattice vector of the atom i in the P unit cell. $|\varphi_i\rangle$ is the atomic orbit of the ith atom and C_i is the expansion coefficients.

The element of the $2N \times 2N$ matrix Hamiltonian

can be written as:

$$[H]_{ij} = \sum_{P} \sum_{\boldsymbol{R}_{Li,Pj}} \mathrm{e}^{\mathrm{i}\boldsymbol{k}\cdot\boldsymbol{R}_{Li,Pj}} \langle\varphi_i| H |\varphi_j\rangle \qquad (10)$$

and

$$\langle\varphi_i| H |\varphi_j\rangle = \begin{cases} \underset{|\boldsymbol{R}_{Li,Pj}|=b}{\rightarrow} \begin{cases} \underset{(i,j)\in \text{edgebond}}{\rightarrow} r_1 + \Delta r, \\ \underset{(i,j)\in \text{others}}{\rightarrow} r_1, \end{cases} \\ \underset{|\boldsymbol{R}_{Li,Pj}|=c}{\rightarrow} r_3, \end{cases} \qquad (11)$$

where $\boldsymbol{R}_{Li,Pj}$ is the distance between the atom i in the L unit cell and the atom j in the P unit cell. The bulk band structure can then be calculated by the Hamiltonian matrix. The complex band structure calculation scheme will be compared with the bulk band structure calculation scheme.

3. Results and discussions

Three parts will be shown in this Section. First, the complex band structure will be compared with the bulk band structure calculations. And second, we will examine the complex band structure of three armchair GNRs. Typical parameters, i.e., the band gap and the maximum imaginary wave vector length, will be examined finally. The simulations are performed using four models to examine the effects of the edge bond relaxation and the third nearest neighbour interaction. Model 1 is the simple tight binding model considering only the first nearest neighbour interaction, and in Eq. (4), we impose the condition that the edge bond relaxation and the third nearest neighbour interaction terms are equal to zero, i.e., $\Delta r = r_3 = 0$ (in order to avoid divergence, we set r_3 equal to a very small value). In Model 2, we consider the edge bond relaxation and set $\Delta r = -0.2$ eV, but still do not consider the third nearest neighbour interaction, i.e., $r_3 = 0$. In Model 3, we consider the third nearest neighbour interaction: $r_3 = -0.3$ eV, but still do not consider the edge bond relaxation, i.e., $\Delta r = 0$. In Model 4, we consider both effects: for edge bond relaxation, we have $\Delta r = -0.2$ eV, and for the third nearest neighbour interaction, we have $r_3 = -0.3$ eV.

In Fig. 2, we show the real band structure calculation results by the transfer matrix method compared with a simple tight binding Hermitian matrix method. Here only the first subband of GNRs is shown. The lines with circles are the real part of the complex band structure. The solid lines are the bulk band structure of GNRs. As expected, the real part of the complex band structure is in good agreement with bulk band structure calculation for all four models with or without the edge bond relaxation and the third nearest neighbour interaction.

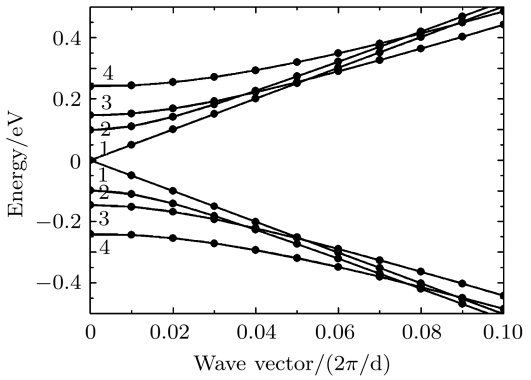


Fig. 2. The real part of the complex band structure calculated by the transfer matrix method (lines with circles) fits well with the bulk band structure calculated by a Hermitian matrix (solid lines). We use $N = 5$ armchair GNR as an example. Here only the first subband is shown. Lines marked by 1 are calculated by simple tight binding model that considers only the first nearest neighbour interaction. Lines marked by 2 are the models considering the edge bond relaxation. Lines marked by 3 are the models considering the third nearest neighbour interactions. And lines marked by 4 are the models considering both the edge bond relaxation and the third nearest neighbour interaction.

We then show the complex band structure calculations for $N = 5$, 6 and 7 armchair GNRs. In Fig. 3, we plot out the complex band structure for $N = 5$ armchair GNRs. The results of the complex band structure calculations from the four models are shown by solid, dot–dash, dot–dot–dash and dot line separately. The imaginary part appears to be a loop connecting the conduction and valence band of GNRs and describes the evanescent behaviour of the band gap states. Unlike carbon nanotubes, edge physics plays an important role in electronic properties of GNRs. The results clearly indicate the importance of the edge bond relaxation and the third nearest neighbour interaction on the band structure of GNRs. For $N = 5$ armchair GNRs, the edge bond relaxation opens a band gap, which is further enlarged by the third nearest neighbour interaction. For $N = 6$ armchair GNRs (in Fig. 4), the band gap is decreased due to the edge bond relaxation and the third nearest neighbour interaction. It has a much smaller imaginary loop, which means an even smaller decay constant. The effective

mass at the band edge is decreased, which means an even higher mobility.

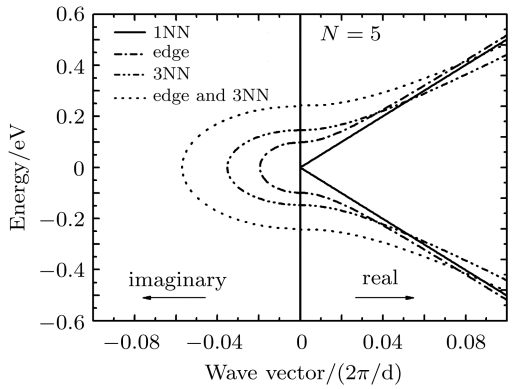


Fig. 3. The complex band structures of $N = 5$ armchair GNR. Here only the first subband is shown. In this plot, the real part of the complex band structure is on the right hand side, and the imaginary part is on the left hand side. The solide line shows the simple first nearest neighbour complex band structure. The dot–dash line shows the results when we only consider the effect of the edge bond relaxation. The dot–dot–dash line shows the results when we consider the effect of the third nearest neighbour. The dot line shows the results when we consider the effects of both the edge bond relaxation and the third nearest neighbour. Due to the edge bond relaxation and the third nearest neighbour interaction, it opens a band gap.

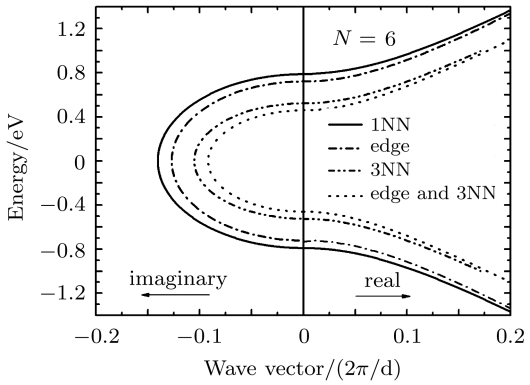


Fig. 4. The complex band structures of $N = 6$ armchair GNR. The solide line shows the simple first nearest neighbour complex band structure. The dot–dash line shows the results when we consider only the effect of the edge bond relaxation. The dot–dot–dash line shows the results when we considered the effect of the third nearest neighbour interaction. The dot line indicates the results when we consider the effects of both the edge bond relaxation and the third nearest neighbour interaction. The band gap is decreased, and the imaginary loop becomes smaller due to the effects of the edge bond relaxation and the third nearest neighbour interaction.

The complex band structure of the $N = 7$ armchair GNRs is shown in Fig. 5, and the edge bond relaxation affects more on the band structure; while the third nearest neighbour interaction has a smaller effect on the band structure. The band gap does not change much, but the band structure has a larger imaginary loop due to the edge bond relaxation and the third nearest neighbour interaction. This also gives the importance of plotting out the whole complex band structure, i.e., in addition to the information given by the band gap, the complex band structure gives extra information, such as the imaginary decay behaviour as mentioned. A nearly unchanged band gap does not mean an unchanged imaginary loop.

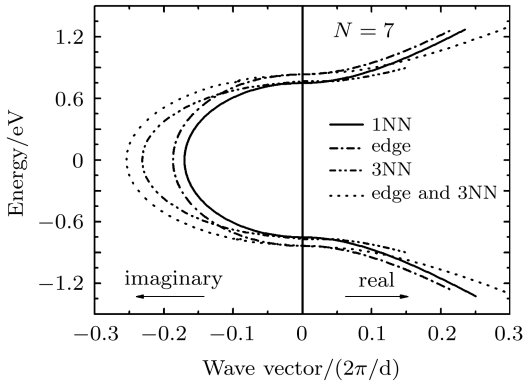


Fig. 5. The complex band structures of $N = 7$ armchair GNR. The solide line shows the simple first nearest neighbour complex band structure. The dot–dash line shows the results when we consider only the effect of the edge bond relaxation. The dot–dot–dash line shows the results when we consider the effect of the third nearest neighbour interaction. The dot line shows the results when we consider the effects of both the edge bond relaxation and the third nearest neighbour interaction. The band gap does not change much, but the imaginary loop becomes larger due to the effects of the edge bond relaxation and the third nearest neighbour interaction.

Figure 6 shows the band gap as a function of the GNRs width number. We find that the GNRs can be discriminated into three distinct families. For $N = 3M - 1$, the effects of the edge bond relaxation and the third nearest neighbour interaction increase the value of band gap. For $N = 3M + 1$, the band gap increase is much smaller than that when $N = 3M - 1$, and for some cases, the band gap is almost unchanged. While, for $N = 3M$, it has the opposite effect, i.e., the band gap becomes smaller. We know that the maximum value of the imaginary wave vector length is important for the understanding of the electron tunnel behaviour through a barrier. Figure 7 gives the maximum value of the imaginary wave vector length as a function of the GNRs width number. As shown in the figure, three distinct family behaviours have also appeared. For $N = 3M - 1$, the effects of edge bond relaxation and the third nearest neighbour interaction enlarge the imaginary loop, and

it has a larger maximum value of imaginary wave vector length. For $N = 3M + 1$, it has similar effect to that when $N = 3M - 1$. While for $N = 3M$, it has the opposite effect, i.e., the imaginary loop becomes smaller.

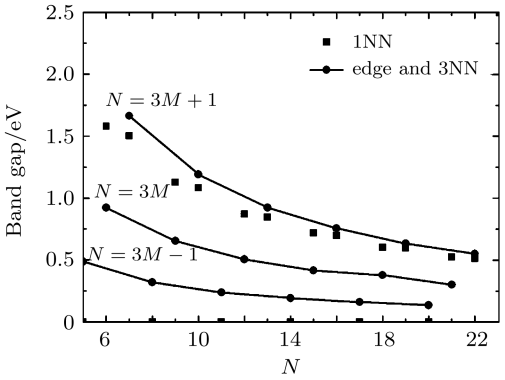


Fig. 6. The band gap of armchair GNRs as a funciton of the GNR width number N. The squares show the results by a simple tight binding model considering only the first nearest neighbour interaction. The lines with circles show the complex band structure calculation results when we consider the effects of both the edge bond relaxation and the third nearest neighbour interaction. The band gap is classified into three familes. The band gap is almost unchanged for the nanoribbons with $N = 3M + 1$.

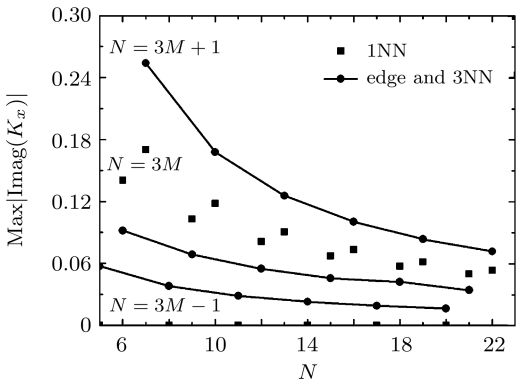


Fig. 7. The maximum value of imaginary wave vector length as a function of the GNRs width number N. The squares show the results when we consider only the first nearest neighbour interaction. The lines with circles show the calculation results when we consider the effects of both the edge bond relaxation and the third nearest neighbour interaction. The maximum value of imaginary wave vector length provides additional information on the electrical characteristics of the armchair GNRs, and is also classified into three familes.

4. Conclusions

This paper presents our study on the complex band structure of armchair GNRs. The complex band structure calculations of the armchair GNRs are performed by the tight binding transfer matrix method including the effects of the edge bond relaxation and the third nearest neighbour interaction. The results are compared with those from the bulk band structure calculations. The bulk band structure is overlapped with the real part of the complex band structure. The imaginary part appears to be a loop connecting the conduction and valence band of GNRs, and describes the evanescent behaviour of the band gap states. As expected, the edge bond relaxation and the third nearest neighbour interaction have profound influence on the complex band structure of GNRs. These calculations may be useful for future design and optimisation of the GNR electronics.

References

[1] Novoselov K S, Geim A K, Morozov S V, Jiang D, Zhang Y, Dubonos S V, Grigorieva I V and Firsov A A 2004 *Science* **306** 666

[2] Zhang Y B, Tan Y W, Stormer H L and Kim P 2005 *Nature* **438** 201

[3] Durkop T, Getty S A, Cobas E and Fuhrer M S 2004 *Nano Lett.* **4** 35

[4] Nakada K, Fujita M, Dresselhaus G and Dresselhaus M S 1996 *Phys. Rev.* B **54** 17954

[5] Barone V, Hod O and Scuseria G E 2006 *Nano Lett.* **6** 2748

[6] Zhou B H, Duan Z G, Zhou B L and Zhou G H 2010 *Chin. Phys.* B **19** 037204

[7] Miyamoto Y, Nakada K and Fujita M 1999 *Phys. Rev.* B **59** 9858

[8] Son Y W, Cohen M L and Louie S G 2006 *Phys. Rev. Lett.* **97** 216803

[9] White C T, Li J, Gunlycke D and Mintmire J W 2007 *Nano Lett.* **7** 825

[10] Reich S, Maultzsch J, Thomsen C and Ordejon P 2002 *Phys. Rev.* B **66** 035412

[11] Brey L and Fertig H A 2006 *Phys. Rev.* B **73** 235411

[12] Lee D H and Joannopoulos J D 1981 *Phys. Rev.* B **23** 4997

[13] Fujita M, Wakabayashi K, Nakada K and Kusakabe K 1996 *J. Phys. Soc. Jpn.* **65** 1920
[14] Gunlycke D and White C T 2008 *Phys. Rev.* B **77** 115116
[15] Yu S S, Wen Q B, Zheng W T and Jiang Q 2008 *Molecular Simulation* **34** 1085
[16] Bowen R C 1995 *Full Bandstructure Modeling of Quantum Transport in Nanoscaled Devices* Ph.D. Thesis The University of Texas at Dallas, Dallas, USA)
[17] Heine V 1965 *Phys. Rev.* **138** A1689
[18] Schulman J N and Chang Y C 1983 *Phys. Rev.* B **27** 2346
[19] Chang Y C and Schulman J N 1982 *Phys. Rev.* B **25** 3975
[20] Tomfohr J K and Sankey O F 2002 *Phys. Rev.* B **65** 245105
[21] Xia T S, Register L F and Banerjee S K 2004 *J. Appl. Phys.* **95** 1597
[22] Xia T S, Register L F and Banerjee S K 2004 *Phys. Rev.* B **70** 045322
[23] Boykin T B 1996 *Phys. Rev.* B **54** 8107
[24] Stóvneng J A and Lipavský P 1994 *Phys. Rev.* B **49** 16494
[25] Bowen R C, Frensley W R, Klimeck G and Lake R K 1995 *Phys. Rev.* B **52** 2754
[26] Ting D Z Y, Yu E T and McGill T C 1992 *Phys. Rev.* B **45** 3583
[27] Mintmire J W and White C T 1995 *Carbon* **33** 893
[28] Lee D H and Joannopoulos J D 1981 *Phys. Rev.* B **23** 4988
[29] Zheng H X, Wang Z F, Luo T, Shi Q W and Chen J 2007 *Phys. Rev.* B **75** 165414
[30] Hu H X, Zhang Z H, Liu X H, Qiu M and Ding K H 2009 *Acta Phys. Sin.* **58** 7156 (in Chinese)
[31] Jin Z F, Tong G P and Jiang Y J 2009 *Acta Phys. Sin.* **58** 8537(in Chinese)